



Published in final edited form as:

Science. 2013 October 11; 342(6155): 212–218. doi:10.1126/science.1238842.

Villification: How the Gut Gets Its Villi

Amy E. Shyer^{1,*}, Tuomas Tallinen^{2,3,*}, Nandan L. Nerurkar¹, Zhiyan Wei², Eun Seok Gil⁴, David L. Kaplan⁴, Clifford J. Tabin^{1,^}, and L. Mahadevan^{2,5,6,7,8,^}

¹Department of Genetics, Harvard Medical School, Boston MA 02115 ²School of Engineering and Applied Sciences, Harvard University, Cambridge MA 02138 ³Department of Physics and Nanoscience Center, University of Jyväskylä, FI-40014 Jyväskylä, Finland ⁴Department of Biomedical Engineering, Tufts University, Medford MA 02155 ⁵Department of Organismic and Evolutionary Biology, Harvard University, Cambridge MA 02138 ⁶Department of Physics, Harvard University, Cambridge, MA 02138 ⁷Wyss Institute for Biologically Inspired Engineering, Harvard University, Cambridge MA 02138 ⁸Kavli Institute for Nanobio Science and Technology, Harvard University, Cambridge MA 02138

Abstract

The villi of the human and chick gut are formed in similar step-wise progressions, wherein the mesenchyme and attached epithelium first fold into longitudinal ridges, then a zigzag pattern, and finally individual villi. We find that these steps of villification depend upon the sequential differentiation of the distinct smooth muscle layers of the gut, which restrict the expansion of the growing endoderm and mesenchyme, generating compressive stresses that lead to their buckling and folding. A quantitative computational model, incorporating measured properties of the developing gut, recapitulates the morphological patterns seen during villification in a variety of species. These results provide a mechanistic understanding of the formation of these elaborations of the lining of the gut, essential for providing sufficient surface area for nutrient absorption.

In amniotes, the primitive midgut is established as a cylinder with an outer mesenchymal layer and an inner, luminal endoderm. As development proceeds, distinct radial layers of smooth muscle differentiate. In parallel, the luminal surface of the gut transforms from a smooth surface to a convoluted morphology. In humans, as well as in mice and birds, this leads to an organized array of finger-like projections termed intestinal villi (1, 2) although a variety of morphologies such as ridges, zigzags, and honeycombs occur in other species (3, 4, 5). Early work suggested a mechanical basis for villus formation (6); however, systematic biological or physical studies of this hypothesis are lacking.

[^]Correspondence should be addressed to: LM LM@seas.harvard.edu. CJT Tabin@genetics.med.harvard.edu.

^{*}These authors contributed equally to this work

Supplementary Materials

Materials and Methods

Supplementary text

Figs. S1 to S11

Movies S1, S2, S3

Morphogenesis and differentiation of the chick midgut

Until embryonic day 7 (E7) the gut tube, with its inner endodermally derived epithelium, and outer mesenchymal layer, maintains a smooth luminal surface (Fig. 1A). However, at E8 as the first layer of circumferentially oriented smooth muscle begins to form, inward buckling of the tube leads to longitudinal ridges that increase in number until E13 when the differentiation of this layer is complete (Fig. 1B). At this point, a second longitudinally oriented layer of muscle differentiates just exterior to the circular layer, while the previously formed ridges fold into parallel zigzags over three days (Fig. 1C). Finally, at E16, as a third, longitudinally oriented muscle layer differentiates just interior to the circular layer, bulges arise from the zigzag pattern that presage the formation of villi (Fig. 1D). The coincident emergence of luminal ridges, zigzags, and villi with the sequential formation of smooth muscle layers, suggests that smooth muscle differentiation and epithelial morphogenesis might be linked.

Ridges form due to muscle-constrained azimuthal growth of the endoderm-mesenchyme composite

The notion that differential growth of layered tissues can lead to epithelial buckling is classical (7, 8), and has been evoked, for example, to explain longitudinal ridge formation in healthy and diseased adult trachea and esophagus (9, 10). To investigate the tissue interactions that lead to the ridge patterns in the embryonic gut, we surgically separated the layers and observed the effects on their respective morphologies. When the muscle was separated from the combined mesenchymal and epithelial layers at different stages from E8, when the circular muscle layer first forms, to E12 just before the first longitudinal muscle layer forms, we found that the mesenchyme and attached epithelium unfold (Fig. 2A). This indicates that as they grew, these layers were under reversible elastic compression when constrained within the muscle layer; indeed the ratio of the inner circumference of the once attached muscle layer to the outer circumference of the separated mesenchyme and endoderm, the circumferential stretch ratio, consistently averages to 0.55 across the developmental stages from E8–E12 (Fig. 2B). However, the separation of the endoderm from the composite of mesenchyme and muscle does not abolish ridge pattern in the mesenchyme (Fig. 2C),

Taken together, these results support a model that the circular muscle layer, once differentiated, forms a stiff constraint mechanically preventing the free azimuthal expansion of the mesenchyme and endoderm; further growth of these tissues relative to the muscle layer leads to azimuthal compression and buckling. This suggests that absent muscle differentiation, the gut tube would expand freely radially without ridge formation. To test this, we developed an *in-vitro* culture system for gut growth. When segments of E6 guts with smooth lumens and no muscle layers are cultured for 48 hours *in vitro*, they differentiate to form a ring of circumferential smooth muscle, and parallel luminal folds, indistinguishable from *in ovo* E8 guts (Fig. 2D). When E6 guts were cultured in the presence of 10 μ M AG1295 or FK506, drugs known to block the differentiation of smooth muscle, but which act through distinct signaling pathways (11, 12), they do not form a smooth muscle layer and concomitantly do not form luminal folds (Fig. 2D). Importantly, these

compounds do not influence proliferation nor lead to an increase in cell death when compared to guts grown with the vehicle (DMSO) alone (Fig. S1); indeed there is a significant increase in the outer circumference of guts lacking circular smooth muscle when compared to control gut samples, confirming that blocking smooth muscle differentiation eliminates circumferential restriction of the outward expansion of the gut tube. As a control, we see that gut segments grown in vehicle alone develop a layer of circular smooth muscle and form luminal folds. Quantifying the constraint provided by the muscle, we find that the ratio of inner circumference of the muscle layer in the control samples to the outer circumference of the gut segments cultured with either compound to be on average 0.53 (Fig. 2D), a ratio that agrees closely with the stretch ratio obtained from surgical separation of the layers, indicating that tissue differentiation into smooth muscle provides most of the circumferential constraint.

Since smooth muscle begins active peristalsis once it forms, the contractility of muscle could drive epithelial buckling in addition to, or instead of, functioning as a passive barrier to expansion. To test this, we cultured E6 gut segments with either sodium nitroprusside (SNP), a compound shown to inhibit smooth muscle contraction during peristalsis, or Motilin, known to enhance peristaltic smooth muscle contraction (13, 14). After 48 hours in culture, neither compound impacted the formation of luminal ridges, suggesting that the spontaneous contractility of smooth muscle is not required for epithelial buckling (Fig. 2E).

Finally, to assess whether the role of the circular smooth muscle layer as a stiff barrier is sufficient to drive luminal folds, we sought to mimic its role in samples where smooth muscle development was blocked. To do so, we constrained radial gut growth using porous silk tubes, synthesized by spinning silk fibroin around a reciprocating rotating mandrel with the inner diameter of the circular smooth muscle (15). E6 gut segments cultured inside of silk tubes in the presence of either AG1295 or FK506 for 48 hours do not form a muscle layer and when given sufficient room to expand in silk tubes of 380 μ m inner diameter, still do not form luminal ridges (Fig. 2F). When the segments are grown in AG1295 and FK506 and restricted by a silk tube of inner diameter of 300 μ m they form ridges similar to those seen in control guts in spite of the lack of smooth muscle (Fig. 2F). This demonstrates that the mechanical barrier function of the circumferential smooth muscle is sufficient for luminal ridge formation. Moreover, upon removal from the confining silk tube, these ridges are quickly lost, just as they vanish from gut tubes upon surgical removal of the circumferential muscle layer (Fig. 2F), corroborating our previous finding that continued mechanical constraint is required for the maintenance of luminal ridges.

Zigzag intermediates form in response to additional muscle-constrained longitudinal growth in endoderm-mesenchyme composite

As described earlier, at E13 a second longitudinally oriented muscle layer forms; simultaneously the ridges buckle into zigzags. Previous work has shown that a thin layer atop an elastic substrate may take on a zigzag topography when it is compressed biaxially (16, 17, 18) suggesting that the longitudinal muscles in conjunction with the previously established circumferential muscle compresses the gut biaxially. To investigate whether the longitudinal muscle layer generates longitudinal compression, we surgically separated the

muscle layers from the endoderm-mesenchyme composite at different developmental stages. At E12, before longitudinal muscle or zigzags have formed, the separated mesenchyme and attached endoderm have approximately the same axial length as the muscle to which it was attached (Fig. 3A). However, after longitudinal muscle layer differentiation, at E13, E14, and E15, the ratio of the length of the separated muscle to mesenchyme and endoderm is approximately 0.75, 0.69, and 0.55 respectively (Fig. 3A), showing that the endoderm-mesenchyme is increasingly compressed longitudinally as this muscle layer forms. Conversely, separation of the endoderm from the mesenchyme and muscle at E14 does not abolish zigzag pattern, suggesting this interaction is not required for maintenance of the zigzags (Fig. 3B).

To directly test whether the development of the outer longitudinal layer is required for the formation of zigzags, we resort again to our *in-vitro* culture system. When E12 gut segments, with a single, circumferential smooth muscle layer and parallel ridges, are cultured for 48 hours, they differentiate a longitudinal smooth muscle layer and undergo morphogenesis to form zigzags, similar to those seen in guts harvested at E14 (Fig. 3C). In the presence of either AG1295 or FK506 the longitudinal muscle layer fails to differentiate, and concomitantly the zigzag pattern does not form suggesting that the longitudinal layer is required to induce zigzags. These compounds only block further smooth muscle formation and leave established layers intact so the ridge patterns remain (Fig. 3C). Additionally, when differentiation of this longitudinal muscle is blocked, the length of the gut increases significantly compared to control gut segments; the ratio of the length of control gut segments to those cultured in the presence of either compound is on average 0.66, i.e. this longitudinal muscle layer compresses the mesenchyme and attached epithelium by a factor of approximately 1.5 (Fig. 3C). This is consistent with the value obtained by manual dissection of the layers. As for ridge formation, transformation of ridges to zigzags is independent of smooth muscle contractility (Fig. S2).

Villification requires a third regime of smooth muscle differentiation

To investigate the dependence of the final patterning of villi on the differentiation of the inner, longitudinal smooth muscle layer, we cultured E15 guts, with both a circumferential layer and outer longitudinal layer, for 48 hours in the presence of the muscle blocking compounds or with the vehicle (DMSO) alone. Although gut segments cultured with DMSO develop a third inner longitudinal muscle layer and form villi, those cultured with either AG1295 or FK506 fail to form this muscle layer and do not initiate villi (Fig. 3D). When differentiation of this longitudinal muscle is blocked, the length of the tube increases significantly compared to control gut segments (Fig. 3D). The ratio of the length of control gut segments to that of those lacking the outer longitudinal muscle is on average 0.68, i.e. this muscle layer compresses the mesenchyme and endoderm again by a factor of approximately 1.5 (Fig. 3D).

All together, our surgical manipulations and drug studies support the hypothesis that differentiating smooth muscle acts as a barrier to the expansion of the attached mesenchyme and endoderm, compressing these layers first circumferentially to form ridges, then longitudinally to form zigzags, and finally longitudinally again to form villi. We emphasize

that since the patterns relax when the muscular constraints are released surgically, it follows that the morphology of the lumen is a simple consequence of elastic energy minimization during the constrained growth of a soft, layered elastic tissue.

Mathematical models quantify the role of tissue growth constrained by muscle layers to drive ridge and zigzag formation

To further quantify these luminal patterns, we constructed a mathematical and computational model of the process based on measured geometrical and biophysical parameters. Our models are similar in spirit to recent theoretical approaches to gut luminal patterning based on the hypothesis of differential growth (19,20), but go beyond them by correctly accounting for the constraints provided by the combination of muscular differentiation and differential growth that we see evidence for, the cylindrical geometry of the gut, and the experimentally measured geometrical and physical properties of the system.

We start by considering a composite of naturally flat elastic mesenchyme and endoderm sheets that are attached together and bend and squeezed to fit into a rigid tubular configuration of inner diameter D that mimics the circular muscle layer (Fig. 4A). We assume that the tissues may be well described using a simple neo-Hookean constitutive model, with a volumetric strain energy density $W = \frac{1}{2}\mu[\text{Tr}(\mathbf{F}\mathbf{F}^T)J^{-2/3} - 3] + K(J - \log J - 1)$, where μ and K are the shear and bulk moduli, respectively, \mathbf{F} is the elastic deformation gradient, and $J = \det(\mathbf{F})$. Over the multi-day timescale of villification, the tissues are assumed compressible with $K = 3\mu$. At each stage, we minimize the elastic energy of the system using a custom finite element model (SI). We characterize growth using the experimentally measured growth parameters, including the outer circumference, $S_0 = \pi D$, of the compressed endoderm-mesenchyme composite, as well as the circumference and thickness of the endoderm and mesenchyme (Figs. 4B and S7). The simulated domain has length $L = 1.25D$ in the longitudinal direction with periodic boundary conditions at the ends, allowing uniform relative longitudinal growth of the layers to develop axial compression that mimics the role of the longitudinal muscles at E13 and E14 when zigzags arise. With the geometrical parameters (full details in SI) and the measured elastic moduli of the tissues (Figs. 4B and S3–S6), which show that the endoderm is approximately 10 times stiffer than the mesenchyme, our simulations allow us to follow the evolution of luminal patterning shown in Fig. 4C and movie S1. We see that both the ridges and zigzag patterns arise as mechanical instabilities in the constrained growing tissue that sequentially break circumferential and then longitudinal symmetry in the gut with a wavelength and amplitude comparable to the thickness of the endoderm-mesenchyme composite (Fig. 4B)

Villification also requires localized changes in endodermal and mesenchymal proliferation in addition to smooth muscle differentiation

Although additional compression from the inner longitudinal layer is necessary for the formation of villi from zigzags, as shown in Figure 3, longitudinal compression alone is not sufficient to effect this transformation (Fig. S9A).

Previous work in mouse has shown that although proliferating cells can be found uniformly across the mesenchyme and endoderm before villi arise, as villi form, proliferating cells are found only in the intervillous region (2). Similarly, in chick guts, proliferating cells appear uniformly within each tissue layer through the formation of zigzags (Figure 5 and S8) but at E15, after zigzags form and just before villi arise, proliferating cells are found predominantly in the valleys between the raised zigzags (Fig. 5A). However, once villi begin to form at E16, proliferation is no longer restricted from the tips (Fig. 5A). Additionally we find that *in vitro* Edu pulse labeling of E15 gut samples results in labeled cells at the sides and tips of forming villi, suggesting these changes in proliferation patterns may reflect a displacement of the dividing cells upward from the valleys as the luminal topography shifts from zigzags to villi. Specifically, each “arm” of the zigzag twists out of the plane and into the lumen, pinching-off a region of the zigzag arm near each “elbow”, delineating pockets of mesenchyme surrounded by endoderm, each of which becomes a villus (Fig. 5B).

To understand how the topographical changes during zigzag twisting might relocate regions of proliferation as villi form, we created a clay model of zigzags. Labeling the proliferating regions of our model zigzags and manually twisted them mimics the twist observed in the E16 gut (Fig. 5C). Furthermore, the resulting clay label localization closely matches Edu staining for proliferation in the sectioned E16 gut tissue (Fig 5C) suggesting that these tissue movements account for the observed proliferation patterns as villi form.

To probe the effect of non-uniform growth in our computational model, we set up a minimal planar configuration of mesenchyme and endoderm (SI, Fig. S9 and movie S2). Initially, the endoderm and mesenchyme are assumed to have nominal compression ratios of 0.5 and 0.6, respectively, in both lateral directions, as measured experimentally (Fig. 3A). This results in a tightly packed zigzag pattern (Fig. S9A), with a spacing of twice the thickness of the endoderm-mesenchyme composite in both directions, in agreement with experiments. Using our experimental observations of non-uniform proliferation as guides, we incorporate non-uniform growth to this pattern by allowing the growth of spots of the endoderm in the zigzag valleys, centered at the deepest points of the valleys, with lateral diameter 6 times the endoderm thickness. These spots are grown laterally until their diameter doubles during the simulation relative to areas of the endoderm outside the spots. This pattern of growth causes the zigzags to shift and twist so as to relocate the rapidly growing regions to the arms, similar to our clay model. As the spots relieve their growth strain at the arms, they form pre-villous bulges (Fig. 5E). Sliced plane views of this twisted pattern reveal show their similarity to the corresponding experimental patterns (Fig. 5F); bulging peaks are rotated while the regular zigzag valleys persist deeper in the pattern.

Thus, although the final patterning step where definitive villi arise involves more complex morphogenesis and non-uniform proliferation, it follows from the same general physical principle: differential growth in a constrained environment leads to buckling and folding patterns as circumferential, longitudinal and eventually radial symmetry are broken sequentially.

A phylogenetically conserved mechanism directs luminal gut morphogenesis

Although the patterns seen on the luminal surface of the gut vary substantially across species (Fig. S10), the underlying physical principles we have uncovered for the chick lumen morphology suggests that similar mechanisms operate broadly.

In the adult *Xenopus*, the luminal surface of the intestine is folded into a zigzag pattern (4). Development of this pattern involves progressing through the same patterning steps as in chick, with a smooth lumen forming ridges that then develop into zigzags via identical mechanisms (Fig. 6A). However, *Xenopus*, unlike chick, does not develop the second inner longitudinal muscle layer (Fig. 6A); the absence of this muscular layer, and thence the absence of additional compression explains why individual villi do not develop in *Xenopus*. Our computational models can account for the differences in zigzags between *Xenopus* and chick, as well as more exotic patterns seen in snakes (SI, Fig. S10).

In the mouse, the gut does not progress through ridges and zigzags and instead, villi emerge directly from a smooth lumen (21). Although these villi arise only once smooth muscle layers form, the layers differentiate much more rapidly in mouse than in chick (Fig. 6E). This suggests that the relatively quick pace at which muscle layers form in the mouse does not leave time for proliferation and expansion of the inner mesenchyme and endoderm in between the differentiation of sequential muscle layers, and thus prevents the development of visible intermediate patterns such as ridges and zigzags. Specifically, all muscle layers develop within a 48 hour period, a short time compared to the 8 days required for muscle to fully develop in chick (21). To experimentally determine whether villus formation in mouse also requires differentiation of smooth muscle, we tested the effect of the smooth muscle inhibitors used in our chick studies on the formation of villi in mouse guts grown in culture. Just as in chick, the mouse guts grown in the presence of AG1295 or FK506 do not form smooth muscle and concomitantly do not develop villi (Fig. 6B), suggesting that compression from the smooth muscle layer is necessary for, and drives the formation of villi in mouse.

Our studies are in sharp contrast to a recent view of mouse gut patterning that postulates a potential inductive role of the endodermally derived signal Sonic Hedgehog (Shh) in triggering a morphogenetic cascade directing villus outgrowth (22). The key results that led in this direction were the failure of villus formation when Shh activity was pharmacologically blocked with the Shh antagonist cyclopamine and the increased size of the villi when guts were provided with excess Shh signal. However, as these reagents were applied prior to villus formation, they were de facto also treated prior to smooth muscle differentiation. As Shh activity is both necessary and sufficient to direct smooth muscle formation in the developing intestine (23, 24), an alternative explanation would be that cyclopamine, by preventing smooth muscle specification, eliminates the constraint necessary for villi to form, consistent with our current studies.

To quantitatively test our theory of villification in the mouse gut, we performed mechanical and morphometric measurements of the tissues in the developing mouse gut (Fig. 6C). Using

these measurements as inputs in our model suffices to quantitatively predict the formation of villi (SI, Figs. 6D and movie S3). Compared to the chick, where the endoderm is more than ten times stiffer than the adjacent mesenchyme, the mouse endoderm is only approximately 1.5 times as stiff as the mesenchyme (Fig. S3). Our simulations show that the soft endoderm in mouse is essential for the initial folding that occurs in endoderm alone, and for the direct formation of an array of pre-villous bumps, rather than zigzags, which are qualitatively similar to sulcus formation on biaxially compressed gel surfaces that lack a stiff top layer (25). The spacing of bumps, and, consequently, the spacing of villi is comparable to the thickness of the whole endoderm-mesenchyme composite (Fig. 6C), similar to chick.

The process of vilification occurs prior to the differentiation of the gut endoderm into various epithelial cell types (26, 27, 28) and well before the post-natal process of crypt formation. Strikingly, *in vitro* culture of intestinal stem cells results in the formation of intestinal organoids which reproduce crypt structure (29). These organoids consist of an inner epithelium with villus-like cell types, and outwardly projecting crypt-like structures. However no morphological structures are present in these *in vitro* cultures resembling the physical villi. These results suggest that crypt formation likely does not require the same muscle-driven compression that is necessary for villi to form.

Additionally, further study is needed to understand whether structural differences in the lumen of different regions of the gut are attributable to distinctions in the parameters we have measured. For example, the short wide villi which coat large longitudinal folds of the chick colon may be attributable to the thicker muscle layers of the colon. Consistent with the muscle playing such a role, studies involving transposition of a ring containing all radial layers of the colon into regions of the small intestine preserve villi morphology (30).

Our previous work provided a mechanical basis for the diversity of macroscopic looping patterns of the gut based on geometry, differential growth, and tissue mechanics (31), and our present results demonstrate the same physical principles drive morphological variation on the luminal surface of the gut. Further, we see that relatively minor changes in the geometry, growth, physical properties and of the developing tissue in the guts of various species can substantially alter both the process and form of villus patterning. A deep understanding of how patterns vary requires us to combine our knowledge of biophysical mechanisms with the genetic control of cell proliferation and growth; indeed this variation can occur in an organism as a function of its diet, across species, and over evolutionary time scales via natural selection.

Supplementary Material

Refer to Web version on PubMed Central for supplementary material.

Acknowledgments

We thank Marc Kirschner for providing *Xenopus* tadpoles and Olivier Pourquie for providing snake embryos. D.L.K. and Tufts University hold a series of patents that cover the processing of silk into material structures, including those utilized in the research reported here. T.T. acknowledges the Academy of Finland for support. Computations were run at CSC – IT Center for Science, Finland. C.J.T acknowledges the support of a grant from the NIH, RO1 HD047360. L.M. acknowledges the support of the MacArthur Foundation.

References

1. McLin VA, Henning SJ, Jamrich M. *Gastroenterology*. 2009; 136:2074–2091. [PubMed: 19303014]
2. Noah TK, Donahue B, Shroyer NF. *Exp Cell Res*. 2011; 317:2702–2710. [PubMed: 21978911]
3. Krause WJ. *Anat Histol Embryol*. 2011; 40:352–359. [PubMed: 21671995]
4. McAvoy JW, Dixon KE. *J Anat*. 1978; 125:155–169. [PubMed: 632211]
5. Ferri S, Junqueira LCU, Medeiros LF, Medeiros LO. *J Anat*. 1976; 121:291–301. [PubMed: 58854]
6. Burgess DR. *Embryol exp Morph*. 1975; 34(3):723–740.
7. His, W. *Anatomie Menschlicher Embryonen*. Vogel: 1880.
8. Moulton DE, Goriely A. *J Mech Phys Solids*. 2011; 59:525.
9. McAvoy JW, Dixon KE. *J Anat*. 1978; 125:155–169. [PubMed: 632211]
10. Bell L, Williams L. *Anat Embryol*. 1982; 165:437–455. [PubMed: 7158824]
11. Kurahashi M, et al. *Neurogastroenterol Motil*. 2008; 20:521–531. [PubMed: 18194151]
12. Fukuda K, Tanigawa Y, Fujii G, Yasugi S, Hirohashi S. *Development*. 1998; 125:3535–3542. [PubMed: 9716519]
13. Benabdallah H, Messaoudi D, Gharzouli K. *Pharmacol Res*. 2008; 57:132–141. [PubMed: 18282715]
14. Harada N, Chijiwa Y, Misawa T, Yoshinaga M, Nawata H. *Life Sci*. 1992; 51:1381–1387. [PubMed: 1383665]
15. Lovett ML, Cannizzaro CM, Vunjak-Novakovic G, Kaplan DL. *Biomaterials*. 2008; 29:4650–4657. [PubMed: 18801570]
16. Bowden N, Brittain S, Evans AG, Hutchinson JW, Whitesides GW. *Nature*. 1998; 393:146–149.
17. Mahadevan L, Rica S. *Science*. 2005; 307:1740. [PubMed: 15774751]
18. Audoly B, Boudaoud A. *J Mech Phys Solids*. 2008; 56:2444–2458.
19. Hannezo E, Prost J, Joanny JF. *Phys Rev Lett*. 2011; 107:78104.
20. Ben Amar M, Jia F. *Proc Natl Acad Sci U S A*. 2013; 110:10525–10530. [PubMed: 23754398]
21. Sbarbati R. *J Anat*. 1982; 135:477–499. [PubMed: 7153168]
22. Walton KD, et al. *Proc Natl Acad Sci U S A*. 2012; 109:15817–15822. [PubMed: 23019366]
23. Sukegawa A, et al. *Development*. 2000; 127:1971–1980. [PubMed: 10751185]
24. Ramalho-Santos M, Melton DA, McMahon AP. *Development*. 2000; 127:2763–2772. [PubMed: 10821773]
25. Tallinen T, Biggins JS, Mahadevan L. *Phys Rev Lett*. 2013; 110:024302. [PubMed: 23383906]
26. Duaca M, et al. *Int J Dev Biol*. 1990; 34:205–18. [PubMed: 2203458]
27. Uni Z, Smirnov A, Sklan D. *Poult Sci*. 2003; 82:320–7. [PubMed: 12619811]
28. Bellware FT, Betz TW. *J Embryol Exp Morphol*. 1970; 24:335–55. [PubMed: 5491984]
29. Sato T, et al. *Nature*. 2009; 459:262–5. [PubMed: 19329995]
30. St Clair WH, Stahlberg CA, Osborne JW. *Virchows Arch B Cell Pathol Incl Mol Pathol*. 1984; 47:27–33. [PubMed: 6151286]
31. Savin T, Kurpios NA, Shyer AE, et al. *Nature*. 2011; 476:57–62. [PubMed: 21814276]

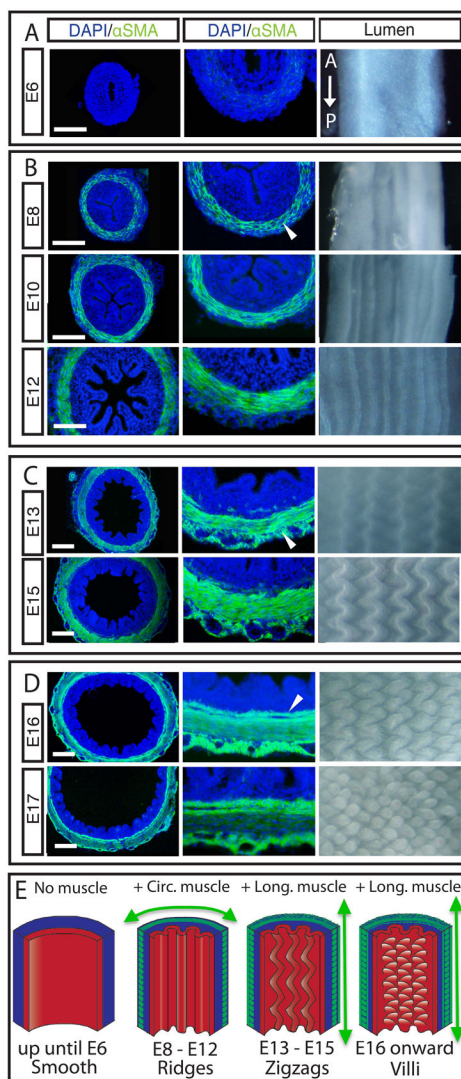


Figure 1. Formation of luminal patterns in chick corresponds with differentiation of smooth muscle layers

Left - Transverse sections of developing chick guts immunostained for nuclei (DAPI, blue) and smooth muscle actin (α SMA, green) during development. Middle - close-up of left panel showing muscle layers. Right - whole mount images of corresponding gut lumen pattern, longitudinal axis runs top to bottom. (A) Lumen is smooth before muscle layers form. (B) Longitudinal ridges form as circularly oriented smooth muscle layer differentiates (arrowhead), and ridge number increases as this layer develops. (C) Longitudinal muscle develops exterior to the circular layer (arrowhead) coincident with the formation of zigzags whose periodicity is maintained but with increasing amplitude and compactness over time. (D) A second longitudinal muscle layer forms, interior to the circular layer (arrowhead), coincident with the formation of villi. (Scale bars = 100 μ m, time is in days past fertilization, e.g. E6). (E) Schematic illustrating the process of muscle differentiation and luminal patterning over time.

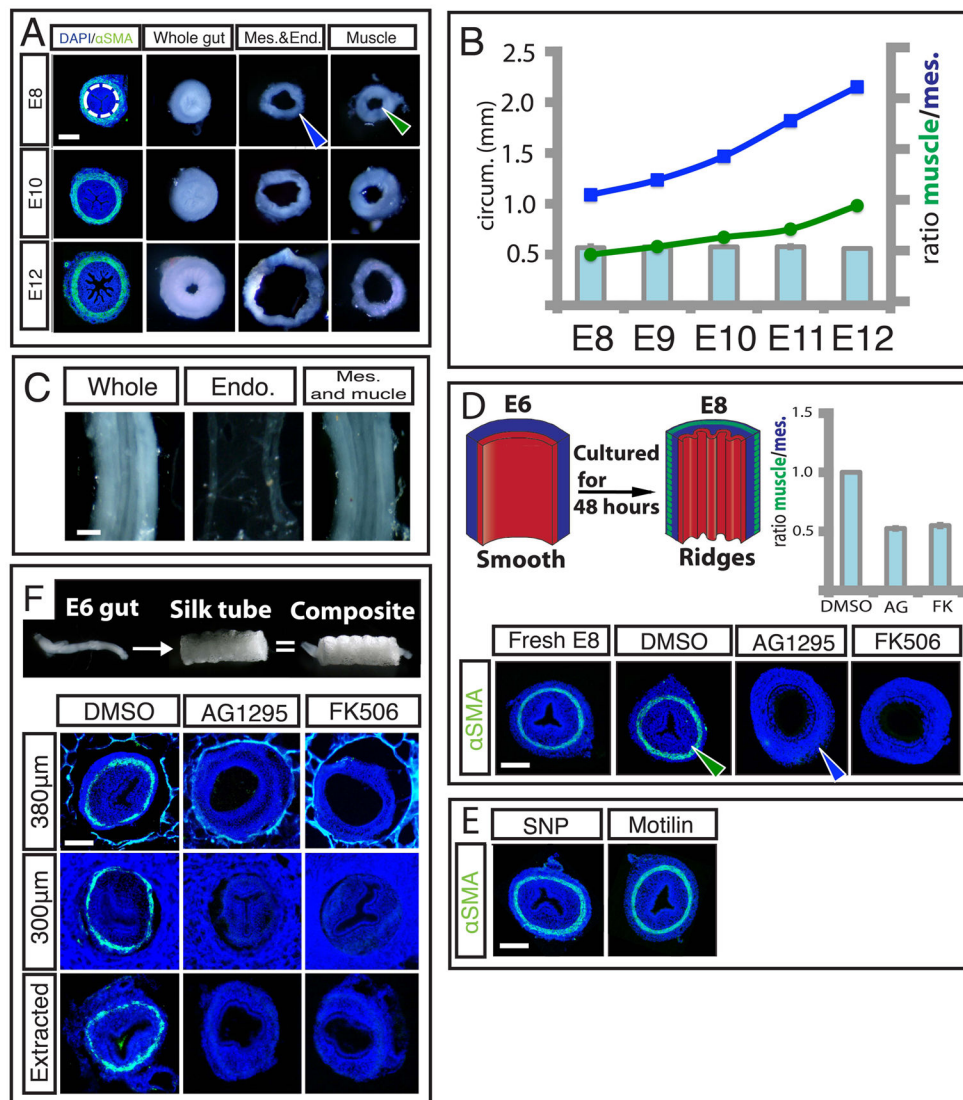


Figure 2. Differentiation of circularly oriented smooth muscle is necessary for maintenance and development of ridges

(A) Transverse slices from E8, E10, E12 whole guts (left) are surgically separated along the junction of the mesenchyme and circular smooth muscle, (dotted line). When separated from the muscle, the luminal ridges in the mesenchyme and attached endoderm unfold (middle) and expand, while the detached muscle remains invariant (right). The outer circumference of the unfolded mesenchyme and endoderm (blue arrowhead) is larger than the inner circumference of the separated muscle layer (green arrowhead) (B) Inner circumference of muscle layer (green line) compared with outer circumference of mesenchyme and endoderm (blue line) over time, along with the compression ratio (bar graph). (C) Surgical separation of endoderm from mesenchyme and muscle at E10 does not abolish ridge pattern. (D) Top left - Experiment schematic of E6 gut cultured for 48 hours. Bottom - Transverse sections of a fresh E8 gut or E6 guts cultured in DMSO alone or with either 10µm AG1295 or 10µm FK506 for 48 hours, labeled with DAPI (blue) and SMA (green), Top right - Quantification of compression from E8 muscle shows the ratio of the inner circumference of the circular

muscle at E8 (green arrowhead) to the resulting mesenchyme outer circumference (blue arrowhead). **(E)** Transverse sections of guts labeled as in D, culturing E6 guts in the presence of either SNP or Motilin does not impact ridge formation. **(F)** Transverse sections of guts labeled as in D, cultured in silk tubes of 380 μ m inner diameter (top), 300 μ m inner diameter (middle), or cultured in 300 μ m and extracted before fixation (bottom). (n > 3 for all culture experiments, error bars represent one SD. Scale bars = 100 μ m)

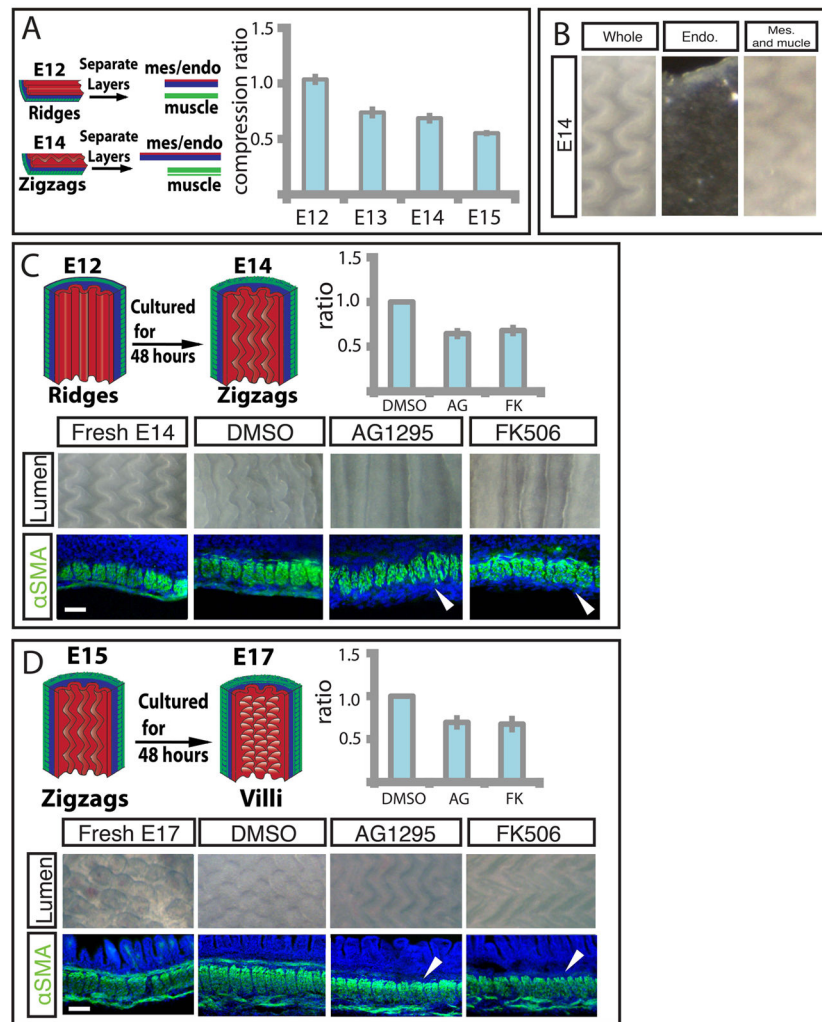


Figure 3. Differentiation of outer and inner longitudinally oriented smooth muscle layers is required for development of the zigzags and villi, respectively

(A) Left - Experimental schematic of tissue separation along the longitudinal axis used to measure longitudinal compression ratio. The muscle (green) from a strip of tissue is dissected away from the mesenchyme (blue)/endoderm (red) and the resulting lengths are compared. Right – Graph of separated muscle layers relative to mesenchyme and attached endoderm before (E12) and after (E13, E14, E15) longitudinal muscle layer forms. (B) Separation of endoderm from mesenchyme and muscle at E14 does not abolish zigzag pattern. (C) Top left panel - Experiment schematic of E12 gut cultured for 48 hours. Bottom - E12 guts cultured in DMSO alone or with either 10 μ m AG1295 or 10 μ m FK506 for 48 hours. Middle panels show luminal views, and bottom panels show longitudinal sections labeled with DAPI (blue) and SMA (green). Arrowhead denotes absence of muscle layer. Top right - Quantification of compression from E14 longitudinal muscle characterized by the ratio of the length of the control cultured segments to those lacking muscle. (D) Top left– Experiment schematic of E15 gut cultured for 48 hours. Bottom - Fresh E17 gut or E15 guts cultured in DMSO alone or with either 10 μ m AG1295 or 10 μ m FK506 for 48 hours. Middle panels show luminal views and bottom panels show longitudinal sections, labeled as

in 3C. Arrowhead denotes absence of muscle layer. Top right - Quantification of compression from E16 longitudinal muscle, as in 3C. ($n > 3$ for all culture experiments, error bars represent one SD. Scale bars = $20\mu\text{m}$)

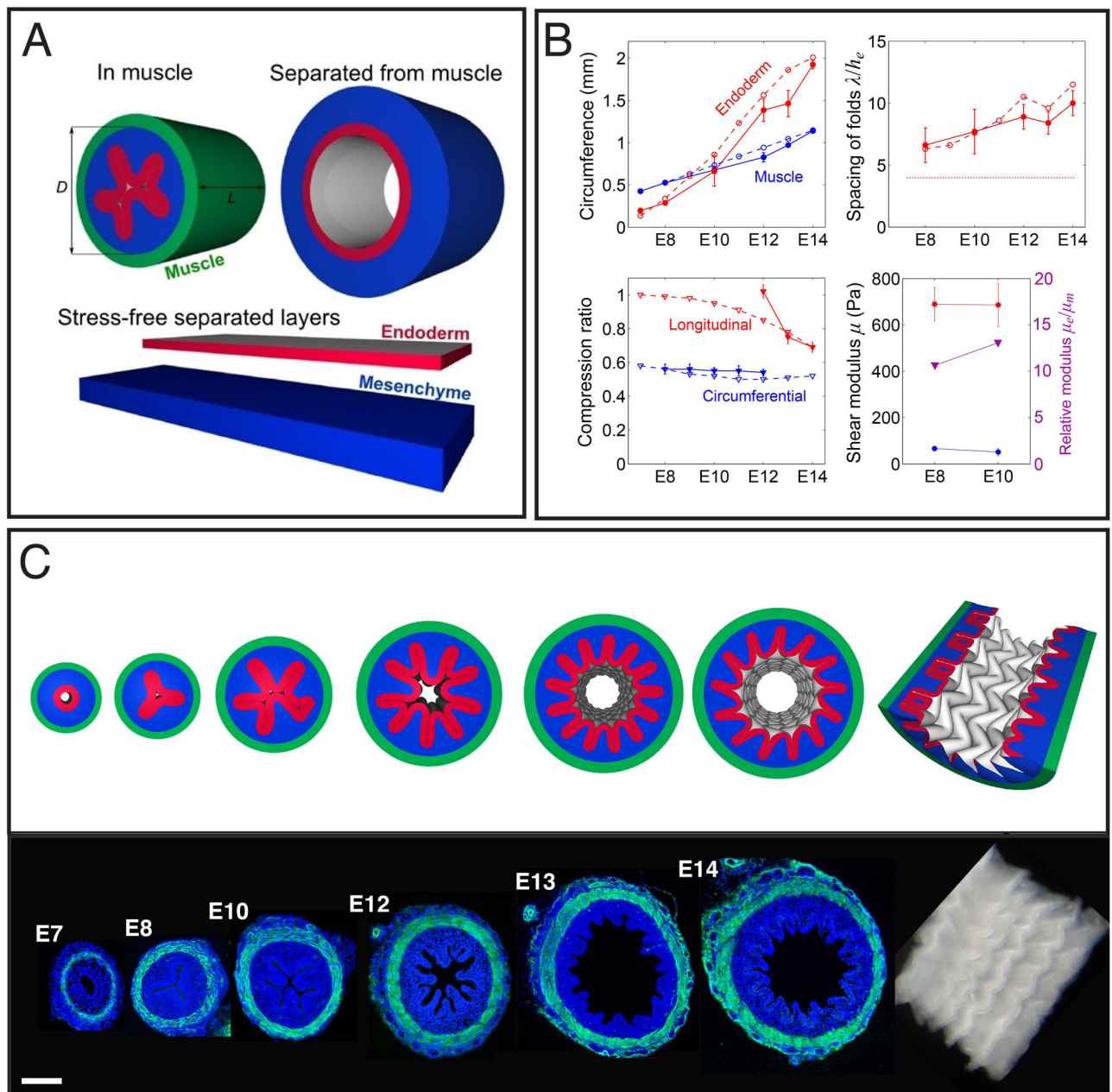


Figure 4. A numerical simulation predicts the formation of ridges and zigzags in chick gut lumen (A) The model is illustrated by showing the mesenchyme (blue) and endoderm (red) enclosed in a muscle (green), without muscle, and separated in their stress-free states. (B) Upper left - Circumference of the inner boundary of the muscle and endoderm. Upper right - Spacing of longitudinal folds measured along the endoderm and scaled by its thickness. The thin dashed line is the stress-free thickness of the endoderm-mesenchyme composite. Lower left - Ratio of muscle to separated endoderm-mesenchyme composite in circumferential and longitudinal directions. Lower right - Shear modulus of mesenchyme and endoderm, and their ratio. In all panels solid lines correspond to experimental observations and dashed lines to the computational model. (C) A simulation shows ridge-folds forming due to

circumferential compression, followed by buckling into a zigzag pattern due to longitudinal compression. Sections of corresponding chick guts labeled with DAPI (blue) and SMA (green) are shown below.

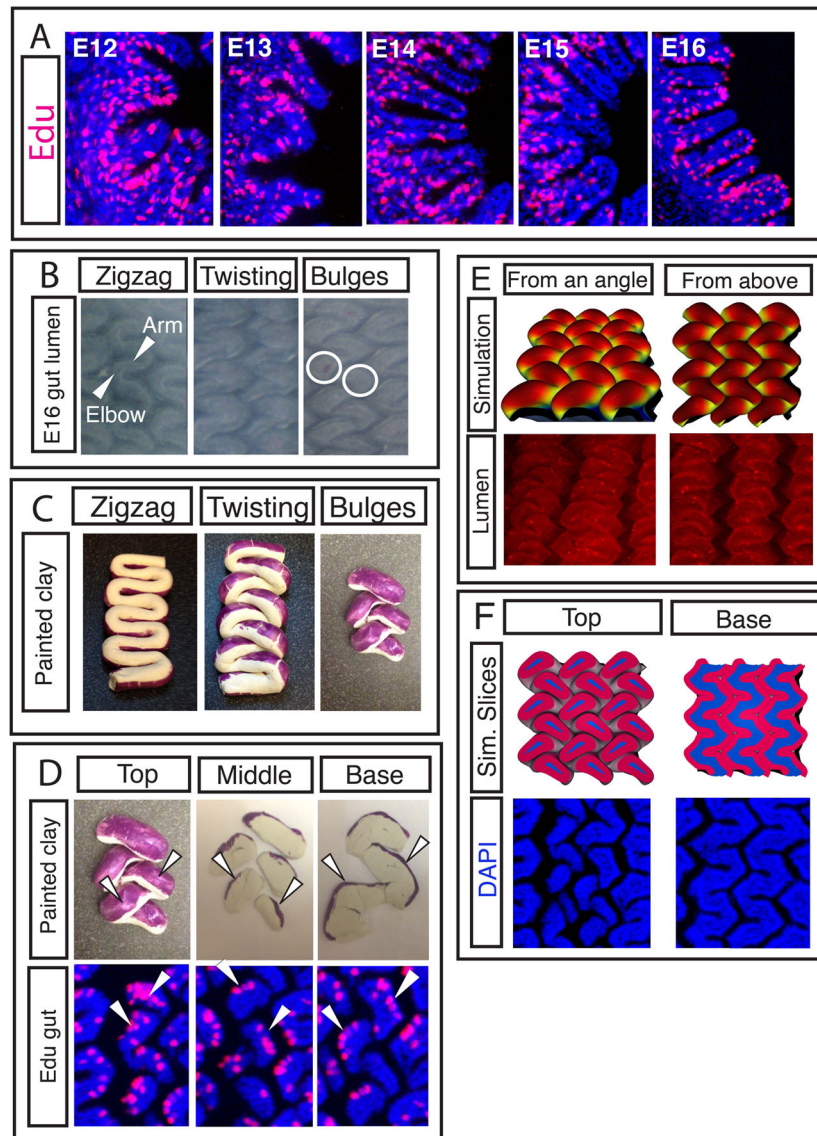


Figure 5. The formation of villi from zigzags involves non-uniform proliferation and a complex change in topography

(A) Transverse sections of guts labeled for 4 hours with Edu in ovo (red) guts show patterns of proliferation over time. (B) Luminal views of guts from E15 to E16 as villi form. The “arm” of the zigzag rotates at the “elbow”, the circles denote the resulting pockets of mesenchyme surrounded by endoderm that will each become a villus. (C) Clay models, purple label represents proliferating regions. Clay model is twisted to mimic change in topography seen in B. (D) Top - Labeled, twisted model of E16 gut is sliced with a razor blade to reveal label localization. Bottom - Edu label in longitudinal sections of E16 guts, arrowheads highlight similarity of pattern. (E) Top - a simulation that incorporates non-uniform proliferation along with measured geometrical and biophysical parameters show villi morphogenesis. Bottom – corresponding images of the chick lumen (red color and stained puncta are due to antibody stain and should be disregarded) (F) Top - sections of the simulations in D. Bottom – corresponding sections in chick.

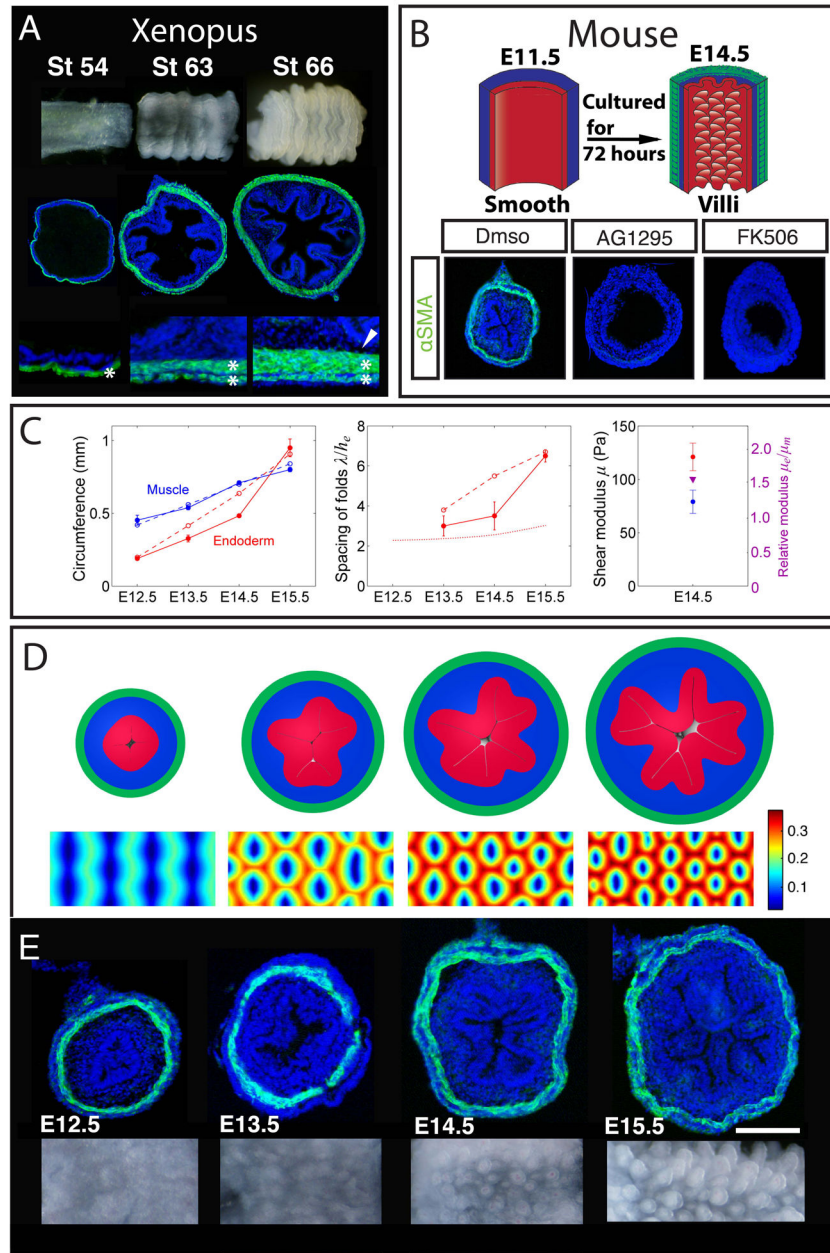


Figure 6. The physical mechanism of villification can be extended to other species
(A) Luminal pattern formation in *Xenopus*. Sections labeled with DAPI (blue) and SMA (green). Here the circumferential and outer longitudinal layer form (asterisks) but the inner longitudinal layer does not form (arrowhead) **(B)** Transverse sections of E11.5 mouse guts (labeled as in A) cultured in vehicle alone (DMSO) or with either 10 μ m AG1295 or 10 μ m FK506 for 72 hours, experiment schematized above. **(C)** Left - circumference of the inner boundary of the muscle and endoderm. Middle - spacing of folds measured along the endoderm and scaled by its thickness. Dotted line is the stress-free thickness of the endoderm-mesenchyme composite. Right - shear moduli of mesenchyme and endoderm, and their ratio. In all panels solid lines correspond to experimental observations and dashed lines

to simulations. **(D)** Cross-sectional (top) and luminal (bottom) images from a simulation based on measurements from the developing mouse gut. Color shows distance of the luminal surface to the center line, relative to the diameter of the tube. **(E)** Transverse sections (labeled as in A) and whole mount images of the lumen for corresponding stages during mouse villi formation. ($n > 3$ for culture experiments, error bars represent one SD. Scale bars = $100\mu\text{m}$)